ADVANCED THERAPEUTICS
www.advtherap.com

Non-Toxic Glycosylated Gold Nanoparticle-Amphotericin B Conjugates Reduce Biofilms and Intracellular Burden of Fungi and Parasites

*Chandradhish Ghosh, Silvia Varela-Aramburu, Hassan E. Eldesouky, Sharareh Salehi Hossainy, Mohamed N. Seleem, Toni Aebischer, and Peter H. Seeberger**

Infections by intracellular pathogens cause significant morbidity and mortality due to lack of efficient drug delivery. Amphotericin B, currently used to treat leishmaniasis and cryptococcosis, is very toxic and cannot eradicate intracellular *Cryptococcus neoformans* (*C. neoformans*). Glycosylated gold nanoparticles are water dispersible and biocompatible with very little toxicity. While amphotericin B is insoluble in water at neutral pH, conjugates of amphotericin B and ultra-small gold nanoparticles (AuNP) are better dispersible in water. Amphotericin B conjugated glycosylated gold nanoparticles (AmpoB@AuNP) are more efficacious in treating both extracellular and intracellular forms of *Leishmania mexicana* (*L. mexicana*) than amphotericin B alone. In addition, AmpoB@AuNP are effective in reducing *C. neoformans* biofilms by 80% and intracellular *C. neoformans* burden by >90%. Furthermore, AmpoB@AuNP are not haemolytic at 50 μg mL^{-1} and are significantly less toxic to murine macrophages than amphotericin B. Ultra-small AuNPs are attractive delivery agents to treat intracellular infections and AmpoB@AuNP may be useful for treating *C. neoformans* infections in immunocompromised patients.

1. Introduction

Infectious diseases are a major contributor to human morbidity and mortality.[1] The utility of antimicrobial agents decreases as pathogens develop resistance against many frontline drugs.[2] Pathogens that survive within mammalian cells are particularly difficult to treat.[3] Pathogens such as *Leishmania spp.* and *C. neoformans* evade phagocytosis before residing and replicating within macrophages that are an important part of the human immune system.[3,4] Treatment of these diseases is challenging as drugs have to enter macrophages before they can exert their anti-infective action.[3,5] Delivery agents that will facilitate the internalization of drugs into specific mammalian cells may be a solution to this problem.

The facultative intracellular pathogen *C. neoformans* causes life-threatening meningitis in patients suffering from AIDS, cancer, autoimmune diseases, and is responsible for around 600 000 deaths globally.[6] Upon inhalation, *Cryptococcus sp.* spores are engulfed by the alveolar macrophages wherein they survive and replicate in mature phagolysosomes. *C. neoformans* disseminates to other organs including the central nervous system.[6a] After crossing the blood brain barrier *C. neoformans* can form biofilms, called cryptococcomas that protects them from host immune defences and antimicrobial therapy.[6a,7]

Dr. C. Ghosh, Dr. S. Varela-Aramburu, Prof. P. H. Seeberger
Department of Biomolecular Systems
Max Planck Institute of Colloids and Interfaces
Am Mühlenberg 1, Potsdam 14476, Germany
E-mail: Peter.Seeberger@mpikg.mpg.de

Dr. S. Varela-Aramburu, Prof. P. H. Seeberger
Institute of Chemistry and Biochemistry
Freie Universität Berlin
Takustraße 3, Berlin 14195, Germany

Dr. H. E. Eldesouky, Prof. M. N. Seleem
Department of Comparative Pathobiology
Purdue University
625 Harrison Street, West Lafayette, IN 47907, USA

Dr. H. E. Eldesouky, Prof. M. N. Seleem
Department of Biomedical Sciences and Pathobiology, Virginia-Maryland College of Veterinary Medicine
Virginia Polytechnic Institute and State University
Blacksburg, VA 24060, USA

S. Salehi Hossainy, Prof. T. Aebischer
Unit 16 Mycotic and Parasitic Agents and Mycobacteria, Department of Infectious Diseases
Robert Koch Institute
Berlin 13353, Germany

The ORCID identification number(s) for the author(s) of this article can be found under https://doi.org/10.1002/adtp.202000293

DOI: 10.1002/adtp.202000293

Therapy against biofilms and intracellular forms of *C. neoformans* is ineffective or drastically reduced.[8,7b] The complications associated with *C. neoformans* infections are a challenging unmet medical need that is being addressed via different paths.[9]

Leishmaniasis, a parasitic tropical disease with high mortality in its most severe form is caused by parasites that exist in two different forms within their host.[10] Extracellular forms called promastigotes are transferred by a sand-fly bite to the host upon a blood meal. These promastigotes are engulfed by phagocytes, in particular, macrophages where they transform to amastigotes and multiply by division. As the disease develops, amastigotes released from host cells are propagated as more and more macrophages become infected. Alternatively, amastigote infected cells are taken up by the sand fly upon biting an infected host, to enter into a new life cycle.

Amphotericin B, the drug used to treat both cryptococcosis and in particular, the severe mucocutaneous and visceral forms of leishmaniasis is poorly water-soluble and quite toxic.[10b] Liposomal formulations of amphotericin B such as AmBisome have reduced its toxicity, but the storage of liposomal formulations is more difficult and costly.[11] To overcome some of these shortcomings, amphotericin B, has been chemically modified, conjugated to polymers,[12] dendrimers,[13] carbon nanotubes,[14] and other nanoparticles.[15] Attempts to improve the solubility of amphotericin B have been made but the toxicity has not been addressed.[16] Recent attempts toward understanding toxicity caused by amphotericin B has led to it being used for other diseases as well.[17] Nevertheless, orally available nanoformulations of amphotericin B remain elusive.[18] More importantly, the drug fails to reduce intracellular infections of *C. neoformans* and their biofilms effectively.

The optical properties of inert and biocompatible[19] gold nanoparticles[20] can be exploited for diagnostic and other applications.[21] Nanoparticulate gold is not toxic to animals[22] and glycosylated-gold nanoparticles[23] are non-toxic and water-soluble.[24] The presence of the sugar not only improves the dispersibility in water but also facilitates further functionalization. Gold nanoparticles can bind to cysteine-rich surface proteins of pathogens due to the affinity for gold to thiols for targeted drug delivery.[25] Here, we show that conjugation of amphotericin B to glycogold nanoparticles renders the drug water dispersible and lowers its toxicity. A significant improvement in drug activity was observed against *L. mexicana* and *C. neoformans*. Unlike amphotericin B, the conjugate was effective in reducing biofilms and intracellular burden of *C. neoformans*.

2. Results and Discussion

2.1. Synthesis and Characterization

The parent gold nanoparticles were prepared by modifying a published protocol.[24] Aurochloric acid was reduced and capped with thioglucose to yield glyco-gold nanoparticles <5 nm according to transmission electron microscopy (TEM) (Figure S1A, Supporting Information). Dynamic light scattering (DLS) revealed hydrodynamic radii of the particles between 10 and 20 nm. The zeta potential for the nanoparticles was determined to be −30 mV (Figure S1B,C, Supporting Information). The thioglucose likely undergoes partial oxidation during the process to yield COOH groups that could be used for further functionalization.

Modification on the mycosamine nitrogen leads to less toxic amphotericin B derivatives without adversely affecting the activity.[26] Thus, it was reasoned that conjugation of amphothericin B to glycogold nanoparticles via the amine group may reduce the toxicity of the drug. The carboxylic acid moieties on the nanoparticles will impart charge to the conjugate and allow for more water molecules to interact with the nanoparticle for better aqueous dispersion. The carboxylic acid groups of the naked glycogold nanoparticles were activated by sonicating AuNP solution with 1-ethyl-3-(3-dimethylaminopropyl)carbodiimide (EDC) and *N*-hydroxysulfosuccinimide (Sulfo-NHS) for five minutes before a solution of amphotericin B in dimethyl sulfoxide (DMSO) was added and sonicated for 2 h (**Scheme 1**). The resultant solution was subjected to dialysis in milliQ water overnight to obtain the amphotericin B-conjugated nanoparticles (AmpoB@AuNP) that were further purified by passing them through a 0.45 µm filter. This solution was characterized using ultraviolet absorption (UV), infrared spectroscopy (IR), DLS, TEM, and atomic force microscopy (AFM).

Amphotericin B is soluble in DMSO and not in water (**Figure 1**A). In comparison, the dispersion of AmpoB@AuNP in water is clear (Figure 1A). UV spectroscopy is an important tool to characterize amphotericin B as it absorbs sharply at 365, 384, and 408 nm in DMSO (Figure 1B). Amphotericin B is not water-soluble, so its UV absorption spectrum in water was not recorded. The suspension of naked gold nanoparticles in water absorbs very little (Figure 1B). The AmpoB@AuNP dispersion in water absorbs at around 325 nm. Both Ambiosome and Fungizone are known to absorb very strongly at 322 nm, which is indicative of the dimeric aggregates of amphotericin B (Figure S1, Supporting Information).[27] In case of AmpoB@AuNP, although the maximum is at 325 nm, other small humps (from 375 to 425 nm) indicated presence of other aggregates (Figure S1, Supporting Information). Similar observations were made with super-aggregates of amphotericin B.[28] However, lyophilization of the water dispersion followed by resuspension in DMSO shows the characteristic peaks of amphotericin B allowing for quantification of the drug conjugated to the nanoparticles (explained below). IR of AmpoB@AuNP reveals distinct peaks at 1654 and 1574 cm^{-1} that represent the carbonyl stretch and N—H bending respectively, convincingly proving the existence of the amide bonds expected from the reaction (Figure 1C). A shoulder at around 1700 cm^{-1} may reflect the free carboxylic acid group of amphotericin B. DLS was used to determine the hydrodynamic radii of the AmpoB@AuNP suspension. (Figure 1D). It was observed that the hydrodynamic radius of the particles increases by 20–30 to ≈45 nm in comparison to the naked gold nanoparticles (≈15 nm, Figure S2B, Supporting Information). The nanoparticles have a ζ potential of the nanoparticles remain similar both before (−30 mV) and after conjugation (−28 mV) confirming their stability in water (Figure 1E and Figure S2C, Supporting Information). TEM analysis of AmpoB@AuNP confirms that the size of the gold clusters is <5 nm (Figure 1F). However, it does not show the actual size of the nanoparticles but only the gold core. AFM was used to visualize and determine the actual particle size. The size of the AmpoB@AuNP varied from 6 to 8 nm, (Figure 1G), while

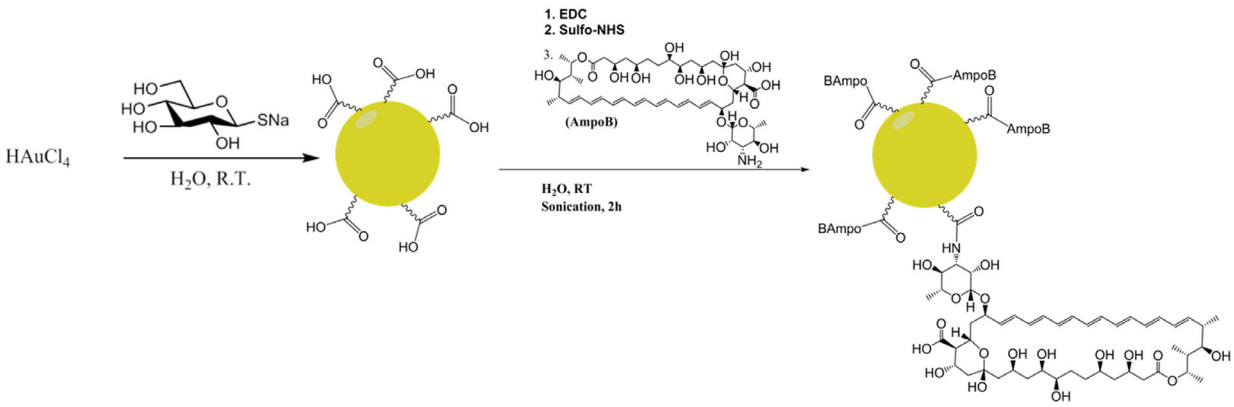

Scheme 1. Synthesis of the amphotericin B—nanoparticle conjugates. (EDC: 1-Ethyl-3-(3-dimethylaminopropyl)carbodiimide; Sulfo-NHS: *N*-hydroxysulfosuccinamide; AmpoB: Amphotericin B. Only one AmpoB in the conjugated form is shown for clarity.)

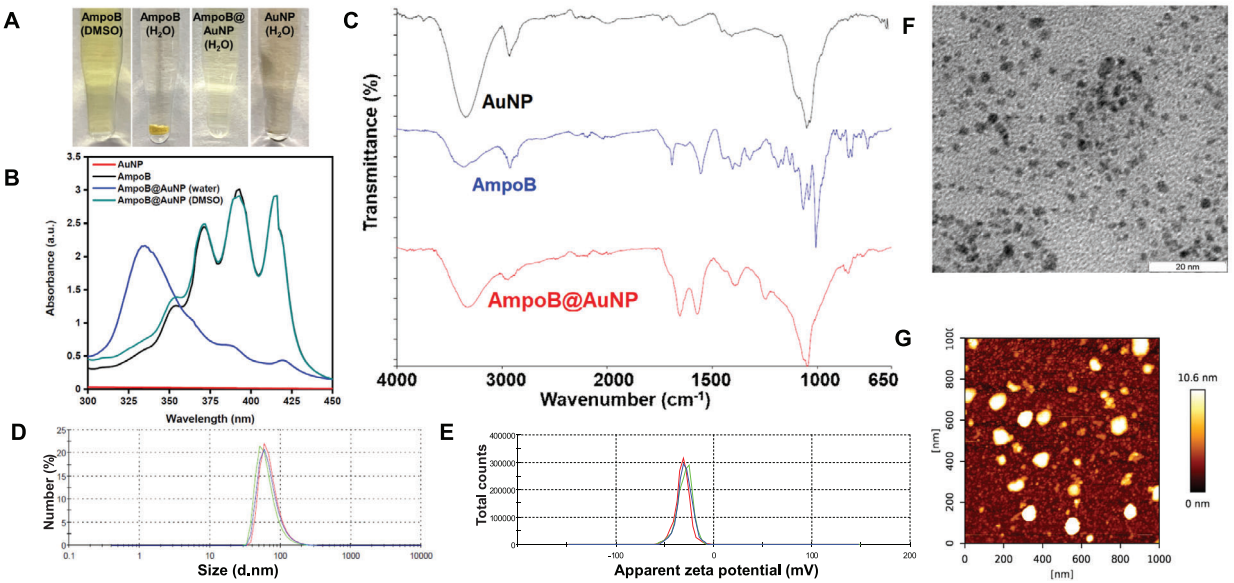

Figure 1. Characterization of AmpoB@AuNP. A) Amphotericin B is soluble in DMSO and insoluble in water, while Ampob@AuNP result in a clear solution. B) UV absorption of the different materials used in the study. AuNP absorbs slightly. For AmpoB in DMSO three distinct peaks are observed at 365, 384, and 408 nm. AmpoB@AuNP do not show signature peaks but have strong absorbance around 340 nm while the same sample in DMSO shows distinct features. C) IR spectra of AmpoB@AuNP shows prominent amide bond peaks at 1654 and 1574 cm^{-1} that are absent in case of Amphotericin B and AuNP. D) DLS measurements indicate that the hydrodynamic radii AmpoB@AuNP are mostly ≈45 nm. E) Zeta potential of AmpoB@AuNP is −28 mV (colored lines represent triplicates in 1D and 1E). F) TEM images of AmpoB@AuNP show the core structure of the gold nanoparticles to be <5 nm (scale bar 20 nm). G) AFM image of AmpoB@AuNP reveals its size to be 6–8 nm.

that of the unconjugated AuNP was 2–3 nm (Figure 1GS2, Supporting Information). This is also clarified by the line scan of the particles (Figure S3, Supporting Information). The synthetic process is reproducible as the nanoparticles maintain similar size, surface, and optical characteristics for each batch. The samples can be stored at 4–8 °C for more than 6 months without significant change in stability or physical properties (based on UV, TEM, DLS, and Zeta potential).

2.2. Quantification of Amphotericin B and Gold Present in the Solution

UV spectroscopy was employed to calculate the amount of amphotericin B present in the suspension. First, the absorbance of amphotericin B was recorded in presence or absence of AuNP (Figure S4A, Supporting Information). Since there was no change in the absorbance it was concluded that the molar absorptivity of amphotericin B in DMSO remained unchanged in presence and absence of AuNP (Figure S3A, Supporting Information). Then different concentrations of amphotericin B (in DMSO) were recorded and plotted to create a standard curve (Figure S4B,C, Supporting Information). Since the absorption spectrum of AmpoB@AuNP in water (Figure 1B) could not be correlated with that of Amphotericin B in DMSO (Figure 1B), AmpoB@AuNP solutions were first lyophilized and then re-suspended in an equal volume of DMSO. The absorbance of this solution was correlated with the concentration of amphotericin B based on the standard curve. (Figure S3, Supporting

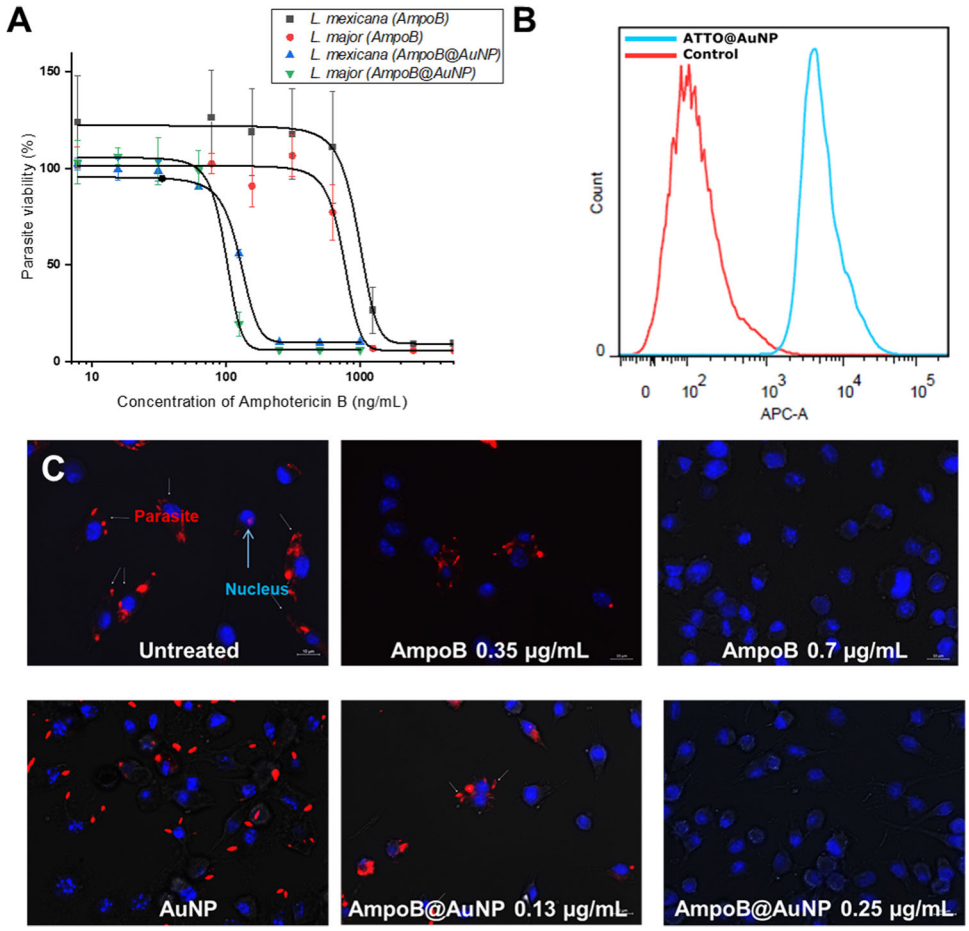

Figure 2. A) Activity of AmpoB@AuNP against metacylcic promastigotes of Leishmania sp. Error bars represent standard deviation values. B) Uptake of ATTO@AuNP nanoparticles by macrophages analyzed by flow cytometry. The shift in the intensity of the fluorescence signal indicates that ATTO@AuNP cells were internalized. The same number of events was recorded. C) Activity against intramacrophage L. mexicana (DSred). Macrophage cells are stained with DAPI and the infected cells are recognized by the red fluorescence of the parasites. Amphotericin B is partly active at 0.35 µg mL^{-1} but completely active at 0.7 µg mL^{-1}. AmpoB@AuNP are partly active at 0.13 µg mL^{-1} while completely active at 0.25 µg mL^{-1}. AuNP do not show inhibition. Error bars represent standard deviation values for triplicates performed using OriginPro 2020b (OriginLab, Northampton, Massachusetts, USA).

Information). The concentration of gold (Au) in the samples was measured using inductively coupled plasma-optical emission spectroscopy. The average ratio between the concentration of amphotericin B and the concentration of gold in the Ampob@AuNP solution (based amount present in µg mL^{-1}) was determined to be 2.5. That corresponds to ≈30 amphotericin B molecules per nanoparticle based on the calculations published previously. For ease of comparison, all activity values are reported in terms of concentration of amphotericinAmphotericin B present in the solution of AmpoB@AuNP as opposed to the concentration of nanoparticles present.

2.3. Activity against Extracellular *Leishmania sp.*

The nanoparticles were checked for activity against the extracellular form of *L. major* and *L. mexicana* parasites and compared to the parent drug. Complete inhibition of cell growth was observed at 250 ng mL^{-1} of AmpoB@AuNP against both *L. mexicana* and *L. major* (**Figure 2**A). The IC_{50} of AmpoB@AuNP was measured at ≈0.1 µg mL^{-1} against *L. major* and ≈0.13 µg mL^{-1} against *L. mexicana* while free drug displayed values between 0.7 and 1 µg mL^{-1} (Figure 2A).

2.4. Intracellular Uptake of Nanoparticles

To study intracellular uptake, AuNPs functionalized with a dye ATTO647N was incubated with macrophages. After washing any surface bound nanoparticles, internalization using flow cytometry was measured. From the flow cytometry analysis, a clear uniform shift in fluorescence intensity of ATTO@AuNP treated cells was observed in comparison to untreated cells confirming the internalization of the particles within macrophages (Figure 2B). Internalization was also observed previously in RBCs.[25]

2.5. Activity against Intracellular *L. mexicana*

The genetically modified *L. mexicana* parasite fluoresces red and can be easily observed under a fluorescence microscope. Upon

Table 1. Summary of antifungal activity.

Fungal isolates	MIC range [μg mL^{-1}]		
	Fluconazole	Amphotericin B	AmpoB@AuNP
Aspergillus sp.	⇒128	2	1
Candida sp.	0.5–>128	0.5–2	0.5–2
Cryptococcus sp.	4–32	1–2	0.5

Unconjugated AuNP was not active.

staining the macrophage nuclei with DAPI, the parasites inside the cell can be easily identified. In the negative control, most of the macrophages (stained blue) contain parasites (stained red) (Figure 2C). Amphotericin B was less effective at 0.35 μg mL^{-1} while no parasites were observed at 0.7 μg mL^{-1}. The IC_{50} of AmpoB@AuNP against extracellular parasites was determined at 0.13 μg mL^{-1}, such that treatment with 0.125 μg mL^{-1}, resulted in some parasite-infected macrophages. At 0.25 μg mL^{-1} of AmpoB@AuNP, no parasites were found within the macrophages illustrating that passive internalization and targeted delivery enhances drug efficacy. Encouraged by these results, the activity of AmpoB@AuNP against fungi was evaluated next.

2.6. Activity against Planktonic Fungi

The minimum inhibitory concentrations (MIC) of amphotericin B, unconjugated gold nanoparticle (AuNP), and AmpoB@AuNP were determined against *Aspergillus sp*., *Candida sp*., and *Cryptococcus sp* to test whether the nanoparticle formulation enhanced the antifungal activity of amphotericin B (**Table 1** and Table S1, Supporting Information). The compounds were tested against three clinical isolates of *Aspergillus sp*. and revealed that AmpoB@AuNP is twice as active (MIC = 1 μg mL^{-1}) as the parent drug (MIC = 2 μg mL^{-1}) (Table 1). AuNP were not active against the pathogens. Activity against *Candida spp*. was tested using four strains of *C. albicans*, five strains of the new emerging multidrug-resistant *C. auris*, four strains of *C. glabrata*, two strains of *C. krusei*, two strains of *C. parapsilosis* and *C. tropicalis*. AmpoB@AuNP were as active as amphotericin B against all the strains of *Candida* except *C. albicans* ATCC 10231, where it was twice more potent than the drug alone.

Next, the compounds were evaluated against *C. gattii* and *C. neoformans*, the causative agents of cryptococcosis, and cryptococcal meningitis (**Table 2**). AmpoB@AuNP were twice more potent than amphotericin B against the four clinical isolates of *C. gattii*. The MIC of AmpoB@AuNP was 0.5 μg mL^{-1} while the unconjugated drug was active at 1 μg mL^{-1}. The two clinical isolates of *C. neoformans* that are resistant to fluconazole require 2 μg mL^{-1} of amphotericin B for activity while AmpoB@AuNP remained active at 0.5 μg mL^{-1}. AmpoB@AuNP were equally or more potent than free amphotericin B against all the fungi that we tested.

2.7. Kinetics of Killing/Antifungal Activity

To assess whether conjugation of amphotericin B to gold nanoparticles alters the rate of killing, the kill kinetics of *C. neoformans* NR41298 with AmpoB@AuNP was determined. The kinetics of the fungicidal activity of AmpoB@AuNP and free amphotericin B were the same at 2 μg mL^{-1} as fungal burden was reduced by five logarithmic scales within 2 h. Free AuNP had no effect on the cells (**Figure 3**A).

Table 2. Antifungal activity against Cryptococcus species.

Fungal isolate	MIC [μg mL^{-1}]		
	Fluconazole	Amphotericin B	AmpoB@AuNP
C. gattii NR-43208	8	1	0.5
C. gattii NR-43209	16	1	0.5
C. gattii NR-43210	16	1	0.5
C. gattii NR-43213	8	1	0.5
C. neoformans NR-41291	16	2	0.5
C. neoformans NR-41295	32	2	0.5
C. neoformans NR-41298	4	1	0.5
C. neoformans NR-48767	4	1	0.5

Unconjugated AuNP was not active.

2.8. Activity against *C. Neoformans* NR-41298 Biofilms

C. neoformans notoriously forms and survives within biofilms, a.k.a. cryptococcomas that are recalcitrant to antifungals and the human immune response. Proteins associated with *C. neoformans* virulence and biofilms contain cysteine-rich regions.[29] Thus, multivalent presentation of the drug and interaction with gold might be able to destroy fungal biofilms more effectively than the unbound drug. Thus, we subjected preformed biofilms of *C. neoformans* to treatment with AmpoB@AuNP and the free drug. Metabolic activity of the biofilms after 24 h indicated that even at concentrations as low as 0.25 μg mL^{-1}, AmpoB@AuNP were able to reduce the burden by 50% while free amphotericin B was not very active at this concentration (Figure S5, Supporting Information). At higher concentrations, the activity of both AmpoB@AuNP and Amphotericin B increased. When treated with 0.5 μg mL^{-1} of AmpoB@AuNP, the metabolic activity of the biofilms was reduced by 75% to further emphasize the potency of AmpoB@AuNP against biofilm infections of *C. neoformans* (Figure 3B). This observation was confirmed by confocal microscopy (Figure S6, Supporting Information). Amphotericin B treated biofilms were stained green (SYTO-9) only and not red (PI), like that negative control and unconjugated gold nanoparticles. On the contrary, significant population of AmpoB@AuNP treated cells were stained red indicative of death (Figure S6, Supporting Information).

2.9. Activity against Intracellular *C. neoformans*

C. neoformans survive and replicate within immune cells. This form of the pathogen is extremely difficult to treat as no dedicated therapeutic is available. Clinically used antifungals are not active against the intracellular form of the pathogen.[8,30] Since AmpoB@AuNP were able to clear *L. mexicana* residing within

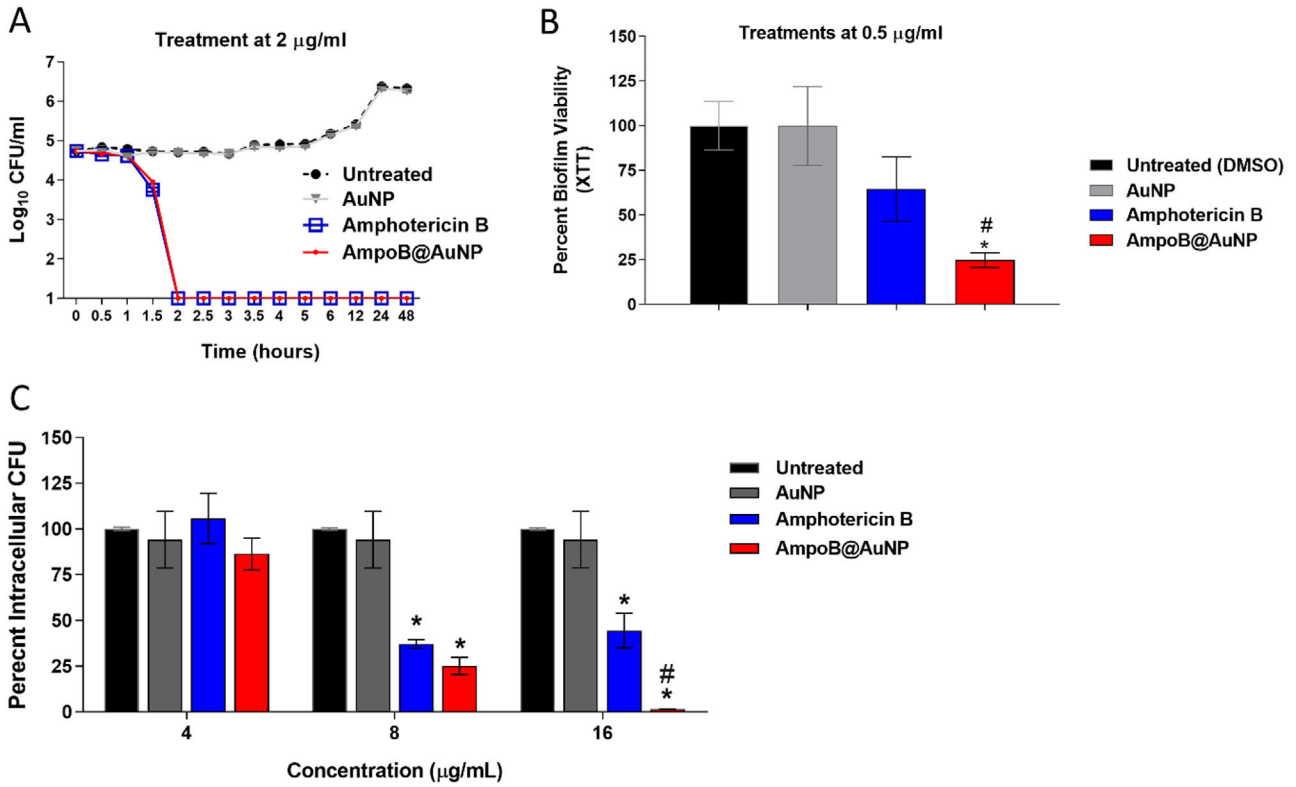

Figure 3. A) Time-kill analysis of Amphotericin B nanoparticles (AmpoB@AuNP) and free Amphotericin B (at 2 μg mL^{-1}) against *C. neoformans* NR-41298 over a 48 h incubation period at 35 °C. DMSO, AuNP served as controls. B) Biofilm eradicating activity of Amphotericin B nanoparticles (AmpoB@AuNP) against *C. neoformans* NR-41298 biofilm evaluated with the XTT assay over a 24-h period. The percent metabolic activity for each treatment was calculated relative to untreated wells. Error bars represent standard deviation values. C) Activity against intracellular *C. neoformans*. Fungal burden of J774 mouse macrophages infected with *C. neoformans* NR-41298, was reduced drastically when treated with AmpoB@AuNP from 8 μg/mL. Amphotericin B is not active. The reduction observed here is partly because of its toxic effect on J774.1 cells. (*) denotes the statistical difference between amphotericin nanoparticles and the untreated control group whereas hash (#) indicates a statistical significance between the amphotericin nanoparticles and the free amphotericin. The statistical significance was assessed with one-way ANOVA, with post hoc Dunnet's multiple comparisons test ($p < 0.05$), utilizing GraphPad Prism 6.0 (GraphPad Software, La Jolla, CA).

macrophages we hypothesized that the intracellular *C. neoformans* can be eradicated by AmpoB@AuNP. At 8 μg mL^{-1} AmpoB@AuNP were able to reduce 75% of the intracellular burden of *C. neoformans* (Figure 3C). AmpoB@AuNP (16 μg mL^{-1}) reduced the fungal burden by more than 90%. The less significant reduction in case of amphotericin B at 8 and 16 μg mL^{-1} was attributed to its cytotoxic effect on the cells.

2.10. Toxicity

Finally, the toxicity of AmpoB@AuNP against mammalian cells was evaluated. The toxicity was evaluated against erythrocytes and the two different murine macrophages used for leishmanial studies and fungal studies (J774.1) respectively (**Figure 4**A–C). Incubation with freshly isolated erythrocytes for 1h revealed that AmpoB@AuNP do not induce visible haemolysis (Figure 4A) even till 64 μg mL^{-1}. Amphotericin B, on the other hand, induces haemolysis at concentrations as low as 6.2 μg mL^{-1} (Figure 4B).

Then, the toxicity of the compounds was evaluated in murine macrophages that served as hosts for *L. mexicana*. LIVE/DEAD staining with a mixture of fluorescein diacetate (FDA) and propidium iodide (PI) was used to determine the toxicity. FDA is a non-fluorescent, cell-permeant dye that is converted to fluorescein intracellularly by esterases expressed by viable cells. The resultant green fluorescence is an indicator of cell-viability. In contrast, PI is non-permeant across cells and stains the nucleus of membrane-compromised cells. When untreated murine macrophages were stained with a mixture of dyes, only green fluorescence was observed (Figure 4C). Upon treatment with Triton X, the cells were compromised allowing PI to stain them red. Similarly, at 16 μg mL^{-1}, amphotericin B was toxic to the cells (mostly red fluorescence is observed) while AmpoB@AuNP were not toxic even at 32 μg mL^{-1} (only green fluorescence was observed). Then, viability of J774.1 cells (the hosts for *C. neoformans*), when treated with different nanoparticles at varying concentrations, was quantified using MTS assay (Figure 4D). Amphotericin B was toxic at concentrations as low as 2 μg mL^{-1}. At 8 μg mL^{-1} amphotericin B treated cells, only 50% of the macrophages remain viable and at 16 μg mL^{-1} almost 80% of the cells are lysed. In comparison, upon treatment with 32 μg mL^{-1} of AmpoB@AuNP, more than 70% of the cells are viable. No toxicity is observed at 16 μg mL^{-1} of AmpoB@AuNP. Thus,

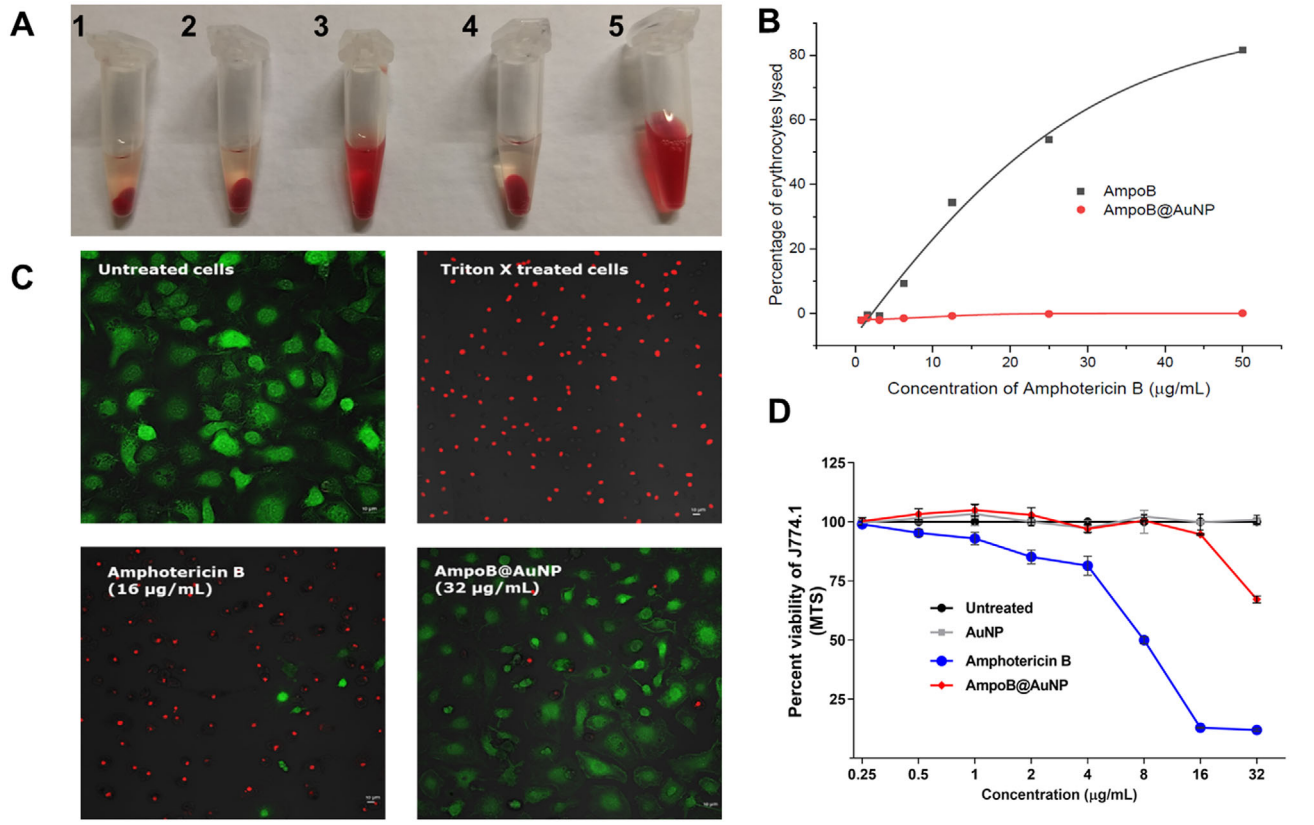

Figure 4. Toxicity of different Amphotericin B formulations. A) Visual representation of haemolysis. 1) Negative control (not haemolytic) 2) AmpoB@AuNP are not haemolytic at concentrations of 64 μg mL^{-1}. 3) Unbound Amphotericin B shows haemolysis even at 12.5 μg mL^{-1} 4) Naked AuNP show no hemolysis and 5) Triton X (positive control) 100% haemolysis. B) Percentage of haemolysis of Amphotericin B and AmpoB@AuNP at different concentrations. C). LIVE/DEAD staining to determine toxicity of AmpoB@AuNP against murine macrophages. Fluorescence microscopy images of macrophage cells after treatment with or without Triton X, Amphotericin B, and AmpoB@AuNP. Staining was performed with fluorescein diacetate (stains intact cells green) and propidium iodide (stains dead cells red). Scale bar 10 μm. D) Toxicity analysis of murine macrophage cells (J774.1) exposed to AmpoB@AuNP, free Amphotericin B, and AuNP for 24 h. Data represent percent viable cells after exposure to the tested treatments at a concentration range 0.25 to 32 μg mL^{-1} using the MTS assay. Dimethyl sulfoxide (DMSO) was used as a negative control. Error bars represent standard deviation values for triplicates performed using GraphPad Prism 6.0 (GraphPad Software, La Jolla, CA).

AmpoB@AuNP have no associated toxicity against mammalian cells at therapeutically relevant concentrations.

3. Conclusion

Multivalent presentation of amphotericin B on ultrasmall nanoparticles renders the formulation dispersible in aqueous media and no loss of activity due to aggregation was observed. Macrophage entry was facilitated due to improved cellular uptake, and less amphotericin B was required for activity while the toxicity was reduced. Although amphotericin B is used as a drug to treat cryptococcosis, it cannot clear biofilms and intracellular forms of *C. neoformans*. The nanogold formulation inhibits all forms of cryptococcal infections at concentrations that are not toxic to the mammalian cells. These glycogold conjugates may be useful for the treatment of intracellular *C. neoformans*.

Supporting Information

Supporting Information is available from the Wiley Online Library or from the author.

Acknowledgements

The authors thank the Max-Planck Society for generous financial support. The authors would also like to thank Eva Settels, Reinhild Dünnebacke, and Rona Pitschke for technical support. The authors would also like to thank Bruna Mara Silva Seco and Dr. Michael Downey for their meticulous scrutiny of the manuscript.

Open access funding enabled and organized by Projekt DEAL.

Conflict of Interest

The authors declare no conflict of interest.

Data Availability Statement

The data that supports the findings of this study are available in the supplementary material of this article.

Keywords

amphotericin B, *Cryptococcus neoformans*, glycogold nanoparticles, intracellular fungi, *Leishmania mexicana*, nanomedicine

Received: December 29, 2020
Revised: February 14, 2021
Published online: March 18, 2021

[1] The top 10 causes of death, https://www.who.int/news-room/fact-sheets/detail/the-top-10-causes-of-death (accessed: July 2019).
[2] D. E. Bloom, S. Black, D. Salisbury, R. Rappuoli, *Proc. Natl. Acad. Sci. USA* **2018**, *115*, 12868.
[3] A. L. Armstead, B. Li, *Int. J. Nanomed.* **2011**, *6*, 3281.
[4] a) N. Abed, P. Couvreur, *Int. J. Antimicrob. Agents* **2014**, *43*, 485; b) C. Coelho, A. L. Bocca, A. Casadevall, *Annu. Rev. Pathol.* **2014**, *9*, 219.
[5] N. F. Kamaruzzaman, S. Kendall, L. Good, *Br. J. Pharmacol.* **2017**, *174*, 2225.
[6] a) L. Aslanyan, D. A. Sanchez, S. Valdebenito, E. A. Eugenin, R. L. Ramos, L. R. Martinez, *J. Fungi* **2017**, *3*, 10; b) R. Rajasingham, R. M. Smith, B. J. Park, J. N. Jarvis, N. P. Govender, T. M. Chiller, D. W. Denning, A. Loyse, D. R. Boulware, *Lancet Infect. Dis.* **2017**, *17*, 873; c) H. Mohammad, N. H. Elghazawy, H. E. Eldesouky, Y. A. Hegazy, W. Younis, L. Avrimova, T. Hazbun, R. K. Arafa, M. N. Seleem, *ACS Infect. Dis.* **2018**, *4*, 403; d) B. J. Park, K. A. Wannemuehler, B. J. Marston, N. Govender, P. G. Pappas, T. A. Chiller, *Aids* **2009**, *23*, 525.
[7] a) L. R. Martinez, A. Casadevall, *Infect. Immun.* **2006**, *74*, 6118; b) L. R. Martinez, A. Casadevall, *Antimicrob. Agents Chemother.* **2006**, *50*, 1021.
[8] J. L. Herrmann, N. Dubois, M. Fourgeaud, D. Basset, P. H. Lagrange, *J. Antimicrob. Chemother.* **1994**, *34*, 1051.
[9] C. Coelho, A. Casadevall, *Cell. Microbiol.* **2016**, *18*, 792.
[10] a) Y. Yeshaw, A. T. Tsegaye, S. G. Nigatu, *Infect. Drug Resist.* **2020**, *13*, 881; b) S. Burza, S. L. Croft, M. Boelaert, *Lancet* **2018**, *392*, 951.
[11] J. P. Adler-Moore, J.-P. Gangneux, P. G. Pappas, *Med. Mycol.* **2016**, *54*, 223.
[12] a) E. Palma, A. Pasqua, A. Gagliardi, D. Britti, M. Fresta, D. Cosco, *Materials* **2018**, *11*, 1167; b) S. Nicoletti, K. Seifert, I. H. Gilbert, *Int. J. Antimicrob. Agents* **2009**, *33*, 441.
[13] K. Jain, A. K. Verma, P. R. Mishra, N. K. Jain, *Nanomedicine* **2015**, *11*, 705.
[14] V. K. Prajapati, K. Awasthi, S. Gautam, T. P. Yadav, M. Rai, O. N. Srivastava, S. Sundar, *J. Antimicrob. Chemother.* **2011**, *66*, 874.
[15] N. Bruni, B. Stella, L. Giraudo, C. Della Pepa, D. Gastaldi, F. Dosio, *Int. J. Nanomed.* **2017**, *12*, 5289.
[16] A. A. Volmer, A. M. Szpilman, E. M. Carreira, *Nat. Prod. Rep.* **2010**, *27*, 1329.
[17] a) T. M. Anderson, M. C. Clay, A. G. Cioffi, K. A. Diaz, G. S. Hisao, M. D. Tuttle, A. J. Nieuwkoop, G. Comellas, N. Maryum, S. Wang, B. E. Uno, E. L. Wildeman, T. Gonen, C. M. Rienstra, M. D. Burke, *Nat. Chem. Biol.* **2014**, *10*, 400; b) K. A. Muraglia, R. S. Chorghade, B. R. Kim, X. X. Tang, V. S. Shah, A. S. Grillo, P. N. Daniels, A. G. Cioffi, P. H. Karp, L. Zhu, M. J. Welsh, M. D. Burke, *Nature* **2019**, *567*, 405.
[18] T. T. Pham, P. M. Loiseau, G. Barratt, *Int. J. Pharm.* **2013**, *454*, 539.
[19] R. Shukla, V. Bansal, M. Chaudhary, A. Basu, R. R. Bhonde, M. Sastry, *Langmuir* **2005**, *21*, 10644.
[20] M. Shah, V. D. Badwaik, R. Dakshinamurthy, *J. Nanosci. Nanotechnol.* **2014**, *14*, 344.
[21] K. Saha, S. S. Agasti, C. Kim, X. Li, V. M. Rotello, *Chem. Rev.* **2012**, *112*, 2739.
[22] J. Xu, M. Yu, C. Peng, P. Carter, J. Tian, X. Ning, Q. Zhou, Q. Tu, G. Zhang, A. Dao, X. Jiang, P. Kapur, J. T. Hsieh, X. Zhao, P. Liu, J. Zheng, *Angew. Chem., Int. Ed. Engl.* **2018**, *57*, 266.
[23] F. Compostella, O. Pitirollo, A. Silvestri, L. Polito, *Beilstein J. Org. Chem.* **2017**, *13*, 1008.
[24] S. Varela-Aramburu, R. Wirth, C. H. Lai, G. Orts-Gil, P. H. Seeberger, *Beilstein J. Nanotechnol.* **2016**, *7*, 1278.
[25] S. Varela-Aramburu, C. Ghosh, F. Goerdeler, P. Priegue, O. Moscovitz, P. H. Seeberger, *ACS Appl. Mater. Interfaces* **2020**, *12*, 43380.
[26] E. Borowski, N. Salewska, J. Boros-Majewska, M. Serocki, I. Chabowska, M. J. Milewska, D. Zietkowski, S. Milewski, *Med. Chem.* **2020**, *16*, 128.
[27] R. Espada, S. Valdespina, C. Alfonso, G. Rivas, M. P. Ballesteros, J. J. Torrado, *Int. J. Pharm.* **2008**, *361*, 64.
[28] a) J. Barwicz, S. Christian, I. Gruda, *Antimicrob. Agents Chemother.* **1992**, *36*, 2310; b) Q. Zia, O. Mohammad, M. A. Rauf, W. Khan, S. Zubair, *Sci. Rep.* **2017**, *7*, 11873; c) Q. Zia, O. Mohammad, M. A. Rauf, W. Khan, S. Zubair, *Sci. Rep.* **2017**, *7*, 11873.
[29] R. Gyawali, S. Upadhyay, J. Way, X. R. Lin, *Appl. Environ. Microb.* **2017**, *83*, e02967.
[30] a) A. Butts, L. DiDone, K. Koselny, B. K. Baxter, Y. Chabrier-Rosello, M. Wellington, D. J. Krysan, *Eukaryotic Cell* **2013**, *12*, 278; b) L. S. Joffe, R. Schneider, W. Lopes, R. Azevedo, C. C. Staats, L. Kmetzsch, A. Schrank, M. Del Poeta, M. H. Vainstein, M. L. Rodrigues, **2017**, *8*, 535.